Experimental Spectroscopic (FTIR, FT-Raman), NBO and NLO Studies of 4, 5-Diphenylimidazole by DFT Method

S.Jaya[1], K.Anitha[2], B. Raja[3] and V. Balachandran[4]

[1]Department of Physics, Periyar EVR College (Autonomous), Tiruchirappalli 620 023, India.
[2]Department of Physics, Bharathidasan university constituent college, Lalgudi, Tiruchirapalli 621 601,India.
[3]Department of Physics, Government Arts College, Kulithalai 639 120, Karur, India.
[4]Department of Physics, A. A. Government Arts College, Musiri 621 211, India.

ARTICLE INFO

ABSTRACT

This work presents the quantum chemical calculations and spectral techniques of 4, 5-Diphenylimidazole (DPI). The spectroscopic properties were investigated by FT-IR and FT-Raman. The FT-IR spectrum (4000–400 cm^{-1}) and FT-Raman spectrum (3500–100 cm^{-1}) in solid phase was recorded for DPI. The optimised geometry, harmonic vibrational frequencies have been investigated by DFT/B3LYP method with 6-31G (d) and 6-311G (d, p) basis sets. The difference between the observed and scaled wave number values of most of the fundamental is very small. Stability of the molecule arising from hyper conjugative interactions, charge delocalization has been analyzed using natural bond orbital (NBO) analysis. HOMO and LOMO energies were measured. The electric dipole moment (μ_D) and first hyperpolarizability (β_{tot}) values of the investigated molecule were computed using ab initio quantum mechanical calculations. The calculated results also show that the DPI molecule may have microscopic nonlinear optics (NLO) behavior. Finally molecular electrostatic potential (MEP) also performed.

Introduction

Imidazoles are well known heterocyclic compounds which are common and have important feature of a variety of medicinal agents. Imidazole is a 5-membered planar ring, which is soluble in water and other polar solvents. It exists in two equivalent tautomeric forms because the hydrogen atom can be located on either of the two nitrogen atoms. It is a highly polar compound, as evidenced by a calculated dipole of 3.61D, and is entirely soluble in water. The compound is classified as aromatic due to the presence of a sextet of π-electrons, consisting of a pair of electrons from the protonated nitrogen atom and one from each of the remaining four atoms of the ring. Imidazole is amphoteric, *i.e.* it can function as both an acid and as a base. On the basis of various literature survey, as a kind of organic low-molecular-weight heterocyclic compounds, imidazole and its derivatives are widely used in a good many domains such as luminescence materials [1], dyesensitized solar cell [2], biomimetic model compounds for the bridging histidine group in superoxide dismutase (SOD) [3] and sequence-specific detection of DNA [4] etc. More importantly, because they can coordinate strongly with transition metals, especially with copper [5], the imidazole derivatives can be applied as treatment agents for metal surfaces [6].

Due to greater pharmaceutical and industrial importance, DPI has been taken for the present study. To our knowledge, no theoretical density functional theory calculations have been performed on DPI. A detailed quantum chemical study will aid in understanding the vibrational modes of this title compound. Hence, the goal of this work is to obtain information about the interactions of 4, 5-diphenylimidazole of the optimized geometrical parameters, vibrational assignments, certain non-linear optical properties (such as dipole moment, polarizability and hyperpolarizability) are analyzed. The redistribution of

electron density (ED) in various bonding, anti-bonding orbitals and E (2) energies had been calculated by natural bond orbital (NBO) analysis to give clear evidence of stabilization originating from the hyper conjugation of various intra-molecular interactions. The HOMO - LUMO analysis have been used to elucidate information regarding charge transfer within the molecule.

Experimental techniques

The newly synthesized compound DPI at Lancaster Chemicals Ltd., UK was purchased and used it for spectral measurements without any further purification. The mid-Infrared (MIR) spectra of the title compound in KBr pellets has been recorded with a NEXUS 670 model of spectrophotometer equipped Mercury-Cadmium-Telluride (MCT-B) as a detector and signal to noise ratio <10. This recorded MIR spectrum in the region 4000–400 cm^{-1} has taken for the vibrational assignments of characteristic group frequencies. Since some of the peaks are IR inactive, we have taken Raman spectra of a molecule in the region 3500–100 cm^{-1} on a NEXUS 670 model of spectrophotometer equipped with Indium-Gallium- Arsenide (InGaAs) detector. While taking FT-Raman, the Nd:YAG laser is used as an excitation source in the FT-Raman module. It emits continuous-wave laser energy at wavelength of 1064 nm and it has a power level of 0.9W at the sample.

Computational details

The optimized molecular structure of DPI (a non planar molecule), belong to C1 point group symmetry. The geometrical parameters for the structure of title molecule in the ground state were optimized at DFT/B3LYP level theory using the 6-31G (d) and 6-311G (d, p) basis set. The vibrational wavenumbers of the compound have also been calculated to improve the simulation of the theoretical spectra. The optimized geometrical parameters, fundamental vibrational frequencies are calculated theoretically

Tele:
E-mail addresses: brsbala@rediffmail.com

using GAUSSIAN 09W package [7]. The theoretical results have enabled us to make the detailed assignments of the experimental IR and Raman spectra of the molecules. The vibrational modes are assigned on the basis of Total Energy Distribution (TED) analysis using Vibrational Energy Distribution Analysis (VEDA) program [8]. By combining the result of the GAUSSVIEW program [9] with symmetry considerations, vibrational frequency assignments are made with a high degree of confidence.

Results and discussions

Molecular geometry

The molecular structure of 4, 5-diphenylimidazole belongs to C1 point group symmetry. The optimized molecular structure of title molecule is obtained from GAUSSIAN 09W and GAUSSVIEW programs with the atom numbering scheme given in Fig. 1 The comparative optimized geometrical parameters (bond lengths and bond angles) calculated by B3LYP (6-31G(d) and 6-311G(d,p)) basis sets are listed in Table 1. Since the geometry of the molecule obtained by B3LYP/6-311G (d, p) method is energetically most stable, hence the theoretical values of this method are taken for correlation and is more reliable.
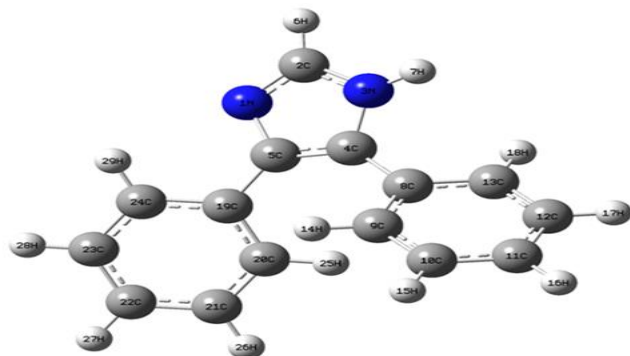
Fig 1. Optimised geometric structure of the DPI compound

Vibrational spectral analysis

The DPI molecule consists of 29 atoms. So, there are 81 vibrational modes. The 81 vibrational modes of DPI have been assigned according to the detailed motion of the individual atoms. The experimental FT-IR and FT-Raman along with the calculated wavenumbers are given in Table 2. The experimental FT-IR and FT-Raman spectra are shown in Figs.2 and 3.
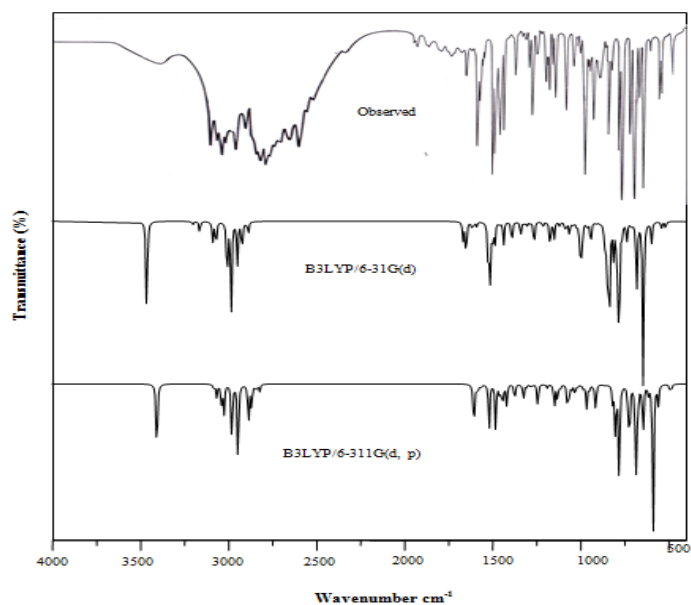
Fig 2. Observed FT-IR and simulated spectra of 4, 5-Diphenylimidazole
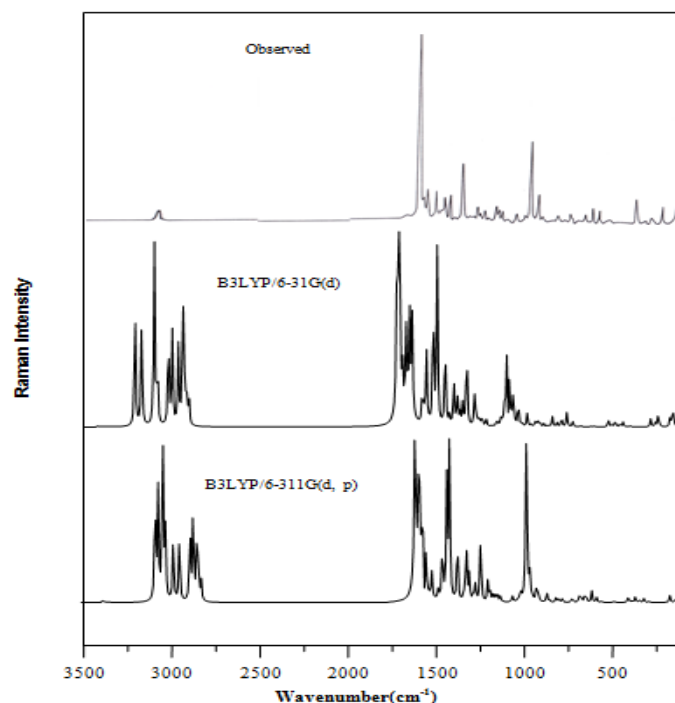
Fig 3. Observed FT-Raman and simulated spectra of 4,5-Diphenylimidazole

Phenyl Ring Vibrations

C–H vibrations

Normally the aromatic ring C–H stretching vibrations are observed in the IR region at 3100–3000cm^{-1} [10]. Similarly, in the phenyl ring C–H stretching vibration was observed at 3082–2820 cm^{-1} in FT-IR and 3062 cm^{-1} at FT-Raman. The TED corresponding to these vibrations with contributions are shown in Table 2. Normally the C–H in plane and out plane bending vibrations occurs in the region 1300–1000 cm^{-1} and 1000–750 cm^{-1} [11, 12] respectively. Additional difficulties may also arise due to the presence of other bands in the region. Hence the C–H in-plane bending of phenyl ring is observed in FT-IR at 1521, 1460,1439, 1373, 1327, 1203, 1176, 1163 and 1073 cm^{-1} and also same region in FT-Raman at 1521, 1479, 1447,1422, 1372, 1340,1192, 1172, 1117 and 1074 cm^{-1}. The C–H out-of-plane bending vibrations are attributed at 1002, 990, 870, 815 and 782 cm^{-1} in FT-IR and 1021, 990, 948, 854,802 and 781 cm^{-1} in FT-Raman. In the present study, the scaled theoretical values of C–H out of plane bending modes calculated at B3LYP/6-311G (d, p) show good agreement with the experimental values of DPI.

C–C vibrations

Aromatic C=C stretching vibrations occur in the region 1625–1430 cm^{-1} and 1150–1070 cm^{-1} [12]. As revealed by TED, the ring C−C stretching modes are observed at 1610,1591, and 1307cm^{-1} in FT-IR and 1604, 1583,1309, 1287 cm^{-1} in FT-Raman for DPI. The in-plane and out-of-plane bending vibrations of the benzene ring are generally observed below 1000 cm^{-1} [13,14] and these modes are not pure but contain a significant contribution from other modes and are substituent-sensitive. In the title molecule, ring in-plane and out-of-plane bending modes are observed at 720, 683, 674, 561, 499 cm^{-1} in FT-IR and 688, 656, 615, 563,485, 369, 292, 177, 122 cm^{-1} in FT-Raman. The scaled theoretical wavenumbers corresponding to ring vibrations are found to have a good correlation with the experimental observations.

Imidazole Ring vibrations

The heteroaromatic molecule containing an N–H group occur in the region 3500–3220 cm^{-1}. The position of absorption in this region depends upon the degree of hydrogen bonding, and

hence upon the physical state of the sample or the polarity of the solvent [10]. In the present work, there is only one N–H stretching modes of imidazole ring observed at 3400 cm^{-1} in FT-IR. Imidazole C–H vibrations are distinctly observed in FT-IR at 3082 cm^{-1} as a strong band. Theoretically predicted wavenumber by B3LYP/6-311G (d, p) at 3083 cm^{-1} is assigned to C–H stretching vibrations. The TED corresponds to this vibration is a pure mode with contribution of 98%. Since the mixing of vibrations of the C–N, C=N with other vibrational modes, the assigning a wavenumber for C–N, C=N vibrations are difficult task. In this present study C–N stretching appears at 1422, cm^{-1} in FT-Raman and 1240 and 1129 cm^{-1} in FT-IR for DPI. These values support the reported results [13,15]. In imidazole ring C−C stretching is observed in 1563 cm^{-1} in FT-Raman and the corresponding theoretical values are 1589 and 1565 cm^{-1} by B3LYP method with 6-31G (d) and 6-311G(d, p) respectively.

Molecular orbitals

Molecular orbitals; both the highest occupied molecular orbital (HOMO) and the lowest unoccupied molecular orbital (LUMO) and their properties such as energy are very useful for physicists and chemists are the main orbital taking part in chemical reaction. While the energy of the HOMO is directly related to the ionization potential, LUMO energy is directly related to the electron affinity [16, 17]. This is also used by the frontier electron density for predicting the most reactive position in p-electron systems and also explains several types of reaction in conjugated system [18]. The conjugated molecules are characterized by a small highest occupied molecular orbital–lowest unoccupied molecular orbital (HOMO–LUMO) separation, which is the result of a significant degree of intramolecular charge transfer from the end-capping electron-donor groups to the efficient electron- acceptor group through-p-conjugated path [19].
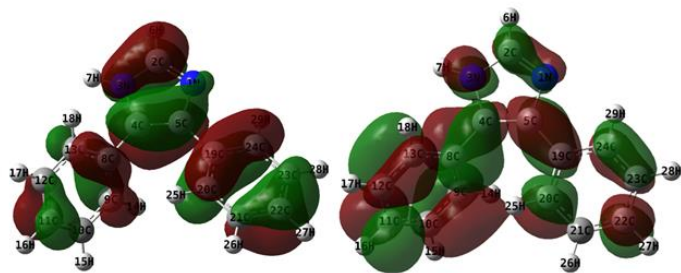
Fig 4. Homo-Lumo of the DPI compound

Surfaces for the frontier orbitals were drawn to understand the bonding scheme of present compound. The energy difference between HOMO and LUMO orbital which is called as energy gap is a critical parameter in determining molecular electrical transport properties because it is a measure of electron conductivity, calculated 4.5941 eV for the title molecule. The plots of MOs (HOMO and LUMO) are drawn and given in Fig.4.The positive phase is red and the negative one is green. According to Fig.4 , the HOMO a charge density localized over the ring of the entire molecule, but the LUMO is characterized by a charge distribution on all structure, expect H atoms. The observed transition from HOMO to LUMO is $\pi \rightarrow \pi^*$. Moreover lower in the HOMO and LUMO energy gap explains the eventual charge transfer interactions taking place within the molecule.

HOMO$_{energy}$ = -5.7942 eV
LUMO$_{energy}$ = -1.2 eV
HOMO - LUMO$_{energy\ gap}$ = 4.5941 eV

Electrostatic potential

It's been pretty well established that the electrostatic potential created by the nuclei and electrons of a molecule in the surrounding space provides a useful tool for interpreting and predicting molecular behaviour. Indeed, it has been shown to be most helpful when studying both electrophilic and nucleophilic processes, and is particularly well suited to studies that involve the identification of key features necessary for the "recognition" of one molecule by another. The molecular surface electrostatic potential (MSEP) is rigorously defined as the first-order interaction between a positive unit charge at any point in the vicinity of a molecule and the charge distribution contributed by both electrons and nuclei. The potential V(r) can be calculated through Equation given below:

$$V(r) = \sum_A \frac{Z_A}{|R_A - r|} - \int \frac{\rho(r)dr'}{|r' - r|}$$

Z_A is the charge on nucleus A located at R_A and $\rho(r)$ is the electron density. The first term in the expression represents the effect of the nuclei and the second represents that of electrons. The two terms have opposite signs and therefore opposite effects. V(r) is their resultant at each point r; it is an indication of the net electrostatic effect produced at the point r by the total charge distribution (electrons + nuclei) of the molecule. Electrostatic potential correlates with dipole moment, electronegativity, partial charges and site of chemical reactivity of the molecule.
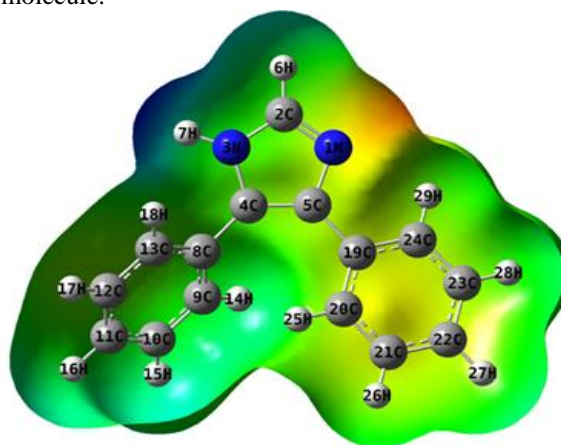
Fig 5. The Molecular electrostaticpotential structure of the DPI compound

The different values of the electrostatic potential at the surface are represented by different colors. Potential increases in the order red < orange < yellow < green < blue. While the negative electrostatic potential corresponds to an attraction of the proton by the concentrated electron density in the molecule (and is colored in shades of red on the ESP surface), the positive electrostatic potential corresponds to a repulsion of the proton by atomic nuclei in regions where low electron density exists and the nuclear charge is incompletely shielded (and is colored in shades of blue). MEP for title molecule is calculated by B3LYP/6-31G (d,p) method as shown in Fig.5 The molecular electrostatic potential (MEP) is related to the electronic density and is a very useful descriptor for determining sites for electrophilic attack and nucleophilic reactions as well as hydrogen-bonding interactions [20, 21]. To predict reactive sites for electrophilic and nucleophilic attack for the title molecule, MEP was calculated at the B3LYP/6-311G(d, p) optimized geometry. The negative (red) regions of MEP were related to electrophilic reactivity and the positive (green) regions to nucleophilic reactivity shown in Fig. 5.

Table 1. Comparison of the geometrical parameters of DPI, bond length (Å) in angstrom and bond angles (º) in degrees by using B3LYP/6-31G(d) and B3LYP/6-311G(d, p)

Bond length(Å)			Bond Angle(º)			Dihedral angle(º)		
Parameter	B3LYP/ 6-31G(d)	B3LYP/ 6-311G (d, p)	Parameter	B3LYP/ 6-31G(d)	B3LYP/ 6-311G(d, p)	Parameter	B3LYP/ 6-31G(d)	B3LYP/ 6-311G (d, p)
N1- C2	1.33	1.32	C2-N1-C5	106.58	106.53	C5-N1- C2-N3	0.12	0.12
N1-C5	1.40	1.40	N1- C2-N3	110.81	110.85	C5-N1- C2- H6	179.93	179.97
C2-N3	1.38	1.37	N1- C2- H6	125.81	125.85	C2-N1- C5- C4	0.65	0.62
C2- H6	1.08	1.07	N3- C2- H6	123.38	123.30	C2-N1- C5- H19	-177.48	-177.72
N3- C4	1.40	1.40	C2-N3- C4	108.25	108.19	N1- C2-N3- C4	-0.84	-0.80
N3- H7	1.01	1.01	C2-N3- H7	126.61	126.69	N1- C2-N3- H7	-175.65	-175.77
C4- C5	1.40	1.39	C4-N3- H7	124.92	124.92	H6- C2-N3- C4	179.34	179.34
C4- C8	1.47	1.47	N3- C4- C5	104.91	104.98	H6- C2-N3- H7	4.53	4.37
C5- H19	1.47	1.47	N3- C4- C8	120.60	120.70	C2-N3- C4- C5	1.18	1.13
C8- C9	1.41	1.41	C5- C4- C8	134.44	134.28	C2-N3- C4- C8	-176.58	-176.87
C8- C13	1.41	1.41	N1- C5- C4	109.43	109.44	H7-N3- C4- C5	176.10	176.21
C9- C10	1.40	1.39	N1- C5- H19	119.72	119.71	H7-N3- C4- C8	-1.66	-1.79
C9- H14	1.08	1.08	C4- C5- H19	130.82	130.83	N3- C4- C5-N1	-1.13	-1.07
C10- C11	1.40	1.40	C4- C8- C9	120.88	120.83	N3- C4- C5- H19	176.73	177.01
C10- H15	1.09	1.08	C4- C8- C13	120.59	120.68	C8- C4- C5-N1	176.18	176.52
C11- C12	1.40	1.40	C9- C8- C13	118.49	118.47	C8- C4- C5- H19	-5.97	-5.40
C11- H16	1.09	1.08	C8- C9- C10	120.62	120.65	N3- C4- C8- C9	133.71	132.56
C12- C13	1.40	1.40	C8- C9- H14	119.31	119.29	N3- C4- C8- C13	-44.20	-45.59
C12- H17	1.09	1.08	C10- C9- H14	120.07	120.06	C5- C4- C8- C9	-43.27	-44.73
C13- H18	1.09	1.08	C9- C10- C11	120.39	120.37	C5- C4- C8- C13	138.82	137.12
H19-C20	1.41	1.41	C9- C10- H15	119.58	119.61	N1- C5- H19-C20	149.77	149.66
H19-C24	1.41	1.41	C11- C10- H15	120.02	120.02	N1- C5- H19-C24	-28.52	-28.89
C20-C21	1.40	1.40	C10- C11- C12	119.55	119.57	C4- C5- H19-C20	-27.90	-28.26
C20-H25	1.08	1.08	C10- C11- H16	120.23	120.22	C4- C5- H19-C24	153.81	153.19
C21-C22	1.40	1.40	C12- C11- H16	120.23	120.21	C4- C8- C9- C10	-178.35	-178.55
C21-H26	1.09	1.08	C11- C12- C13	120.18	120.18	C4- C8- C9- H14	1.26	1.13
C22-C23	1.40	1.40	C11- C12- H17	120.12	120.12	C13- C8- C9- C10	-0.40	-0.35
C22-H27	1.09	1.08	C13- C12- H17	119.70	119.70	C13- C8- C9- H14	179.21	179.33
C23-C24	1.40	1.40	C8- C13- C12	120.77	120.77	C4- C8- C13- C12	177.92	178.10
C23-H28	1.09	1.08	C8- C13- H18	119.58	119.59	C4- C8- C13- H18	-3.91	-3.62
C24-H29	1.08	1.08	C12- C13- H18	119.63	119.62	C9- C8- C13- C12	-0.03	-0.10
			C5- H19-C20	122.30	122.28	C9- C8- C13- H18	178.13	178.18
			C5- H19-C24	119.24	119.28	C8- C9- C10- C11	0.55	0.54
			C20- H19-C24	118.44	118.42	C8- C9- C10- H15	180.00	179.98
			H19-C20-C21	120.72	120.73	H14- C9- C10- C11	-179.06	-179.14
			H19-C20-H25	119.83	119.82	H14- C9- C10- H15	0.39	0.29
			C21-C20-H25	119.44	119.45	C9- C10- C11- C12	-0.25	-0.26
			C20-C21-C22	120.34	120.33	C9- C10- C11- H16	179.79	179.78
			C20-C21-H26	119.57	119.60	H15- C10- C11- C12	-179.70	-179.70
			C22-C21-H26	120.08	120.07	H15- C10- C11- H16	0.34	0.34
			C21-C22-C23	119.41	119.43	C10- C11- C12- C13	-0.18	-0.19
			C21-C22-H27	120.26	120.26	C10- C11- C12- H17	-179.50	-179.50
			C23-C22-H27	120.33	120.31	H16- C11- C12- C13	179.78	179.77
			C22-C23-C24	120.34	120.34	H16- C11- C12- H17	0.46	0.47
			C22-C23-H28	120.04	120.02	C11- C12- C13- C8	0.32	0.37
			C24-C23-H28	119.62	119.64	C11- C12- C13- H18	-177.84	-177.91
			H19-C24-C23	120.74	120.74	H17- C12- C13-C8	179.65	179.68
			H19-C24-H29	118.61	118.61	H17- C12- C13- H18	1.49	1.40
			C23-C24-H29	120.65	120.64	C5- H19-C20-C21	-179.43	-179.58
						C5- H19-C20-H25	-0.51	-0.62
						C24- H19-C20-C21	-1.12	-1.02
						C24- H19-C20-H25	177.80	177.94
						C5- H19-C24-C23	179.45	179.59
						C5- H19-C24-H29	-0.06	0.18
						C20- H19-C24-C23	1.09	0.98
						C20- H19-C24-H29	-178.42	-178.42
						H19-C20-C21-C22	0.37	0.31
						H19-C20-C21-H26	179.70	179.65
						H25-C20-C21-C22	-178.55	-178.65
						H25-C20-C21-H26	0.77	0.69
						C20-C21-C22-C23	0.43	0.45

						C20-C21-C22-H27	179.90	179.90
						H26-C21-C22-C23	-178.89	-178.89
						H26-C21-C22-H27	0.58	0.56
						C21-C22-C23-C24	-0.46	-0.48
						C21-C22-C23-H28	179.39	179.38
						H27-C22-C23-C24	-179.94	-179.93
						H27-C22-C23-H28	-0.09	-0.07
						C22-C23-C24- H19	-0.31	-0.24
						C22-C23-C24-H29	179.19	179.15
						H28-C23-C24- H19	179.84	179.90
						H28-C23-C24-H29	-0.66	-0.71

Table 2. The second order perturbation energies E(2) (kcal/mol) corresponding to the most important charge transfer interactions (donor - acceptor) in the DPI studied by B3LYP/6-311G(d,p) method

Donor	ED(i)e	Acceptor(j)	ED(j)e	E(2) (kcal/mol)	E(i)- E(j) (arb.units)	F(i,j) (arb.units)
π(N 1 - C 2)	1.8766	π*(C 4 - C 5)	0.3884	17.9	0.33	0.074
σ(N 1 - C 5)	1.9478	σ*(C 5 - C 19)	0.0411	10.95	1.95	0.131
σ(N 3 - C 4)	1.9612	σ*(C 4 - C 8)	0.0411	9.38	1.98	0.122
σ(C 4 - C 5)	1.8945	σ*(C 4 - C 8)	0.0411	15.28	1.82	0.151
σ(C 4 - C 5)	1.8945	σ*(C 5 - C 19)	0.0411	13.23	1.84	0.141
π(C 4 - C 5)	1.7285	π*(N 1 - C 2)	0.0097	21.81	0.21	0.063
σ(C 4 - C 8)	1.9417	σ*(C 4 - C 5)	0.1080	13.56	1.47	0.128
σ(C 4 - C 8)	1.9417	σ*(C 8 - C 9)	0.0584	13.96	1.5	0.129
σ(C 4 - C 8)	1.9417	σ*(C 8 - C 13)	0.0584	14.15	1.5	0.13
σ(C 5 - C 19)	1.9418	σ*(C 4 - C 5)	0.1080	13.18	1.46	0.125
σ(C 5 - C 19)	1.9418	σ*(C 19 - C 20)	0.3864	13.9	1.5	0.129
σ(C 5 - C 19)	1.9418	σ(C 19 - C 24)	0.0553	14.05	1.5	0.13
σ(C 8 - C 9)	1.9332	σ*(C 4 - C 8)	0.0411	16.61	1.87	0.159
σ(C 8 - C 13)	1.9339	σ*(C 4 - C 8)	0.0411	16.28	1.88	0.157
π(C 8 - C 13)	1.6210	π*(C 9 - C 10)	0.3139	20.08	0.27	0.066
π(C 8 - C 13)	1.6210	π*(C 11 - C 12)	0.3320	21.61	0.27	0.068
π(C 9 - C 10)	1.6657	π*(C 8 - C 13)	0.3960	21.14	0.29	0.071
π(C 9 - C 10)	1.6657	π*(C 11 - C 12)	0.3320	20.55	0.28	0.067
π(C 11 - C 12)	1.6565	π(C 8 - C 13)	1.6210	18.69	0.29	0.067
π(C 11 - C 12)	1.6565	π(C 9 - C 10)	1.6657	20.45	0.28	0.068
σ(C 19 - C 20)	1.9334	σ*(C 5 - C 19)	0.0411	16.48	1.88	0.158
π(C 19 - C 20)	1.6113	π*(C 21 - C 22)	0.3364	22.46	0.26	0.069
π(C 19 - C 20)	1.6113	π*(C 23 - C 24)	0.3154	20.3	0.26	0.066
π(C 21 - C 22)	1.6607	π*(C 19 - C 20)	0.3864	18.18	0.3	0.067
π(C 21 - C 22)	1.6607	π*(C 23 - C 24)	0.3154	20.35	0.28	0.068
π(C 23 - C 24)	1.6675	π*(C 19 - C 20)	0.3864	20.96	0.3	0.072
π(C 23 - C 24)	1.6675	π*(C 21 - C 22)	0.3364	20.76	0.28	0.068
LP(1) N 3	1.6043	π*(N 1 - C 2)	0.4104	37.27	0.27	0.09
LP(1)N 3	1.6043	π*(C 4 - C 5)	0.3884	26.97	0.34	0.086
π*(N 1 - C 2)	0.4104	π*(C 4 - C 5)	0.3884	26.71	0.07	0.061
π*(C 9 - C 10)	0.3139	π*(C 8 - C 13)	0.3960	186.51	0.02	0.082
π*(C 11 - C 12)	0.3320	π*(C 8 - C 13)	0.3960	174.6	0.02	0.08
π*(C 21 - C 22)	0.3364	π*(C 19 - C 20)	0.3864	128.55	0.02	0.08
π*(C 23 - C 24)	0.3154	π*(C 19 - C 20)	0.3864	144.9	0.02	0.083

Table 3. The values of calculated μ_D, α and β_{tot} components for DPI by B3LYP/6-31G(d) and B3LYP/6-311G(d, p) method

Parameter	B3LYP/6-31G(d)	Parameters	B3LYP/6-311G(d,p)
μ_x	3.7142	βxxx	79.4279
μ_y	-0.9064	βxxy	247.0677
μ_z	-0.3164	βxyy	236.5901
μ_D	3.8363	βyyy	4.8651
αxx	172.9067	βxxz	-4.5263
αxy	-3.3576	βxyz	11.2837
αyy	164.209	βyyz	-11.9693
αxz	-5.1634	βxzz	45.3634
αyz	-4.4599	βyzz	-5.7234
αzz	139.2814	βzzz	3.5401
α(esu)	2.3534×10^{-23}	β_{tot} (esu)	3.7795×10^{-30}
$\Delta\alpha$(esu)	4.88683×10^{-24}		

The negative regions are mainly localized on the nitrogen N1 in the imidazole ring. Also, a negative electrostatic potential region is observed around the C19, C20, C21, C22, C23 and C24 in the benzene ring. A maximum positive region is localized on the hydrogen atom H7 indicating a possible site for nucleophilic attack. The MEP map shows that the negative potential sites are on electronegative atoms as well as the positive potential sites are around the hydrogen atoms. The MEP provides a visual representation of the chemically active sites and comparative reactivity of the atoms.

Natural bond orbital (NBO) analysis

NBO analysis provides the most accurate possible 'natural Lewis structure' picture of φ, because all orbital details are mathematically chosen to include the highest possible percentage of the electron density. A useful aspect of the NBO method is that it gives information about interactions in both filled and virtual orbital spaces that could enhance the analysis of intra- and intermolecular interactions. The second-order Fock matrix was carried out to evaluate the donor–acceptor interactions in the NBO analysis. The interactions result is a loss of occupancy from the localized NBO of the idealized Lewis structure into an empty non-Lewis orbital. For each donor (i) and acceptor (j), the stabilization energy E(2) associated with the delocalization i →j is estimated as

$$E(2) = \Delta E_{ij} = q_i \frac{F(i,j)^2}{\varepsilon_j - \varepsilon_i}$$

where q_i is the donor orbital occupancy, ε_i and ε_j are diagonal elements and $F(i, j)$ is the off-diagonal NBO Fock matrix element. The NBO bond polarization and hybridization changes were associated with formation of the compound. In NBO analysis, large E (2) value shows the intensive interaction between electron-donors and electron-acceptors and greater the extent of conjugation of the whole system, the possible intensive interactions are given in Table 3.

In NBO analysis, the hyperconjugative σ − σ* interactions play a highly important role. These interactions represent the weak departures from a strictly localized natural Lewis structure that constitutes the primary ''noncovalent'' effects. The intramolecular hyperconjugative interactions are formed by the orbital overlap between σ (C–C) and germinal σ *(C–C) bond orbitals which results intramolecular charge transfer (ICT) causing stabilization of the system are presented in Table 3. The hyperconjugative interaction of σ (C19–C20) distribute to σ * (C5–C19) leading to stabilization energy of 16.48 kcal/mol. The interesting intramolecular hyperconjugative interaction of π

electrons from C19–C20 to the π * antibonding orbital of C21–C22 leading to the stabilization energy of 22.46 kcal/mol. The most important interactions have occurred from the electron donating LP1 (N3) to the antibonding acceptor π *(N1– C2) with stabilization energy 37.27 kcal/mol. This highest interaction around the ring can induce high reactivity in the molecule.

NLO properties

The first hyperpolarizability (β_0) of this novel molecular system and related properties (β_{tot} α, Δα) of DPI are calculated using DFT/B3LYP methods at 6-31G (d) and 6-311G (d, p) basis set based on the finite field approach. In the presence of an applied electric field, the energy of a system is a function of the electric field. First, hyperpolarizability is a third-rank tensor that can be described by a 3 x 3 x 3 matrix. The 27 components of the 3D matrix can be reduced to 10 components due to the Kleinman symmetry. It can be given in the lower tetrahedral format. It is obvious that the lower part of the 3 x 3 x 3 matrixes is a tetrahedral. The components of b are defined as the coefficients in the Taylor series expansion of the energy in the external electric field. When the external electric field is weak and homogeneous, the expansion becomes

$$E(F) = E(0) - \mu_i F_i - \frac{1}{2}\alpha_{ij}F_iF_j - \frac{1}{6}\beta_{ijk}F_iF_jF_k - \frac{1}{24}\gamma_{ijkl}F_iF_jF_kF_l - ....$$

where $E(0)$ is the energy of the unperturbed molecules, F_i is the field at the origin and μ_i, α_{ij} and γ_{ijkl} are the components of dipole moment, polarizability and the first hyperpolarizabilities respectively. The total static dipole moment μ_D, the mean polarizability α, the anisotropy of the polarizability Δα and the mean first hyperpolarizability β_{tot} using the x, y, z components, they are defined as

$$\mu = \left(\mu_x^2 + \mu_y^2 + \mu_z^2\right)^{1/2}$$

$$\langle\alpha\rangle = \frac{\alpha_{xx} + \alpha_{yy} + \alpha_{zz}}{3}$$

$$\Delta\alpha = \left\{\frac{(\alpha_{xx} - \alpha_{yy})^2 + (\alpha_{xx} - \alpha_{zz})^2 + (\alpha_{zz} - \alpha_{yy})^2 + 6(\alpha_{xz}^2 + \alpha_{yz}^2 + \alpha_{xy}^2)}{2}\right\}^{1/2}$$

$$\beta_{tot} = \left[(\beta_{xxx} + \beta_{xyy} + \beta_{xzz})^2 + (\beta_{yyy} + \beta_{yzz} + \beta_{yxx})^2 + (\beta_{zzz} + \beta_{zxx} + \beta_{zyy})^2\right]^{1/2}$$

The total static dipole moment, the mean polarizability, the anisotropy of the polarizability and the mean first-order hyperpolarizability of the title compound have been calculated using B3LYP /6-31G (d) and 6-311G (d, p) levels. The

conversion factor α, β and HOMO and LUMO energies in atomic and cgs units: 1 atomic unit (a. u.) =0.1482 x 10^{-24} electrostatic unit (esu) for α; 1 a.u. = 8.6393 x 10^{-33} esu for β; 1 a.u. = 27.2116 eV (electron volt) for HOMO and LUMO energies.

Urea is one of the prototypical molecule used to compare the study of the NLO properties of the molecular system. Therefore it was used frequently as a threshold value for comparative purposes [22-26]. The calculated dipole moment and hyperpolarizability values obtained from B3LYP/6-311G (d, p) method are collected in Table 4. The total molecular dipole moment of DPI from B3LYP with 6-311G (d, p) basis set is 3.8363Dwhich is 2.8 times greater than the value for urea (μ = 1.3732D). Similarly the first order hyperpolarizability of DPI with B3LYP/6-311G (d, p) basis set is 3.7795 x 10^{-30} esu which is ten times greater than the value of urea ($β_{tot}$ = 0.372 x 10^{-30} esu). From the computation the high values of the hyperpolarizability of DPI are probably attributed to the nonlinear optical (NLO) property of the molecule.

Conclusions

In the present work, the optimized molecular structure, vibrational Frequencies of the title compound have been calculated by DFT method using B3LYP/6-31G(d) and 6-311G(d, p) basis set. The optimized geometric parameters (bond lengths, bond angles and dihedral angles) are theoretically determined. The vibrational FT-IR and FT-Raman spectra of the DPI are recorded and on the basis of agreement between the calculated and experimental results, assignments of all the fundamental vibrational modes of the title compound were made unambiguously based on the results of the TED output. When all theoretical results scanned, they are showing good correlation with experimental data. The differences between the observed and scaled wavenumber values of most of the fundamentals are very small. Therefore, the assignments made at DFT level of theory with only reasonable deviations from the experimental values seem to be correct. The NBO analysis indicates the intramolecular charge transfer between the bonding and antibonding orbitals. NLO properties of the DPI are much greater than those of urea.

References

[1] T.N. Sorrell, A.S. Borovik, J. Am. Chem. Soc. 108 (1986) 2479.

[2] H. Kusama, H. Arakawa, H. Sugihara, J. Photochem. Photobio. A:Chem. 171 (2005) 201.

[3] D.A. Daly, L.L. Martin, Inorg. Chem. Commun. 5 (2002) 777.

[4] K.L. Buchmueller, A.M. Staples, C.M. Howard, S.M. Horick, P.B. Uthe,N.M. Le, K.K. Cox, B. Nguyen, K.A.O. Pacheco, W.D. Wilson, M. Lee,J. Am. Chem. Soc. 127 (2005) 742.

[5] R.J. Sundberg, R.B. Martin, Chem. Rev. 74 (1974) 471.

[6] S. Yoshida, H. Ishida, Appl. Surf. Sci. 20 (1985) 497.

[7] M.J. Frisch, G.W. Trucks, H.B. Schlegal, G.E. Scuseria, M.A. Robb, et al., Gaussian09, Revision A.02, Gaussian, Inc., Wallingford CT, 2009

[8] M.H. Jamroz, Vibrational Energy Distribution Analysis, VEDA Computer Program, Poland, 2004.

[9] A. Frisch, A.B. Nielson, A.J. Holder, GAUSS VIEW Users Manual, Gaussian Inc., Pittsburgh, PA, 2000.

[10] M. Silverstein, G. Clayton Basseler, C. Morill, Spectrometric Identification of Organic Compounds, Wiley, New York, 1981

[11] G. Socrates, Infrared Characteristic Group of Frequencies, Wiley, New York, 1980.

[12] G. Varasanyi, Assignments of Vibrational Spectra of Seven Hundred Benzene Derivatives, Wiley, New York, 1974.

[13] Y. Erdogdu, D. Manimaran, M. T. Güllüoglu, M. Amalanathan, I. Hubert Joe, S. Yurdakul, Optics and Spectroscopy, 114(2013) 525–536.

[14] N.P.G. Roeges, A Guide to the Complete Interpretation of Infrared Spectra of Organic Structures, Wiley, New York, 1994.

[15] M.Karnan, V. Balachandran , M. Murugan, M.K. Murali, Spectrochimica Acta 130 (2014) 143–151.

[16] K. Fukui, Science 218 (1982) 747.

[17]S. Gunasekaran, R.A. Balaji, S. Kumeresan, G. Anand, S. Srinivasan, Can.J. Anal. Sci. Spectrosc. 53 (2008) 149.

[18] K. Fukui, T. Yonezawa, H. Shingu, J. Chem. Phys. 20 (1952) 722.

[19] C.H. Choi, M. Kertesz, J. Phys. Chem. 101A (1997) 3823.

[20] E. Scrocco, J. Tomasi, Adv. Quantum Chem. (1979) 11.

[21] N. Okulik, A.H. Jubert, Internet Electron J. Mol. Des. (2005)4.

[22] Y.X. Sun, Q.L. Hao, Z.X. Yu, W.X. Wei, L.D. Lu, X. Wang, Mol. Phys. 107 (2009) 223.

[23] A.B. Ahmed, H. Feki, Y. Abid, H. Boughzala, C. Minot, A. Mlayah, J. Mol. Struct. 920 (2009) 1.

[24] J.P. Abraham, D. Sajan, V. Shettigar, S.M. Dharmaprakash, N.I.H. Joe, V.S. Jayakumar, J. Mol. Struct. (2009) 917–927.

[25] S.G. Sagdinc, A. Esme, Spectrochim. Acta A 75 (2010) 1370–1376.

[26] A.B. Ahamed, H. Feki, Y. Abid, H. Boughzala, C. Monit, Spectrochim. Acta A 75 (2010) 293–298